TECHNIQUE FOR PROCESSING OF CONTINUOUS CARBON FIBRE REINFORCED PEEK FOR FUSED FILAMENT FABRICATION

Jing Pu[a,b], Ehab Saleh[c], Ian Ashcroft[a], Arthur Jones[b]

[a] Centre for Additive Manufacturing, Faculty of Engineering, The University of Nottingham, Nottingham, NG8 1BB, U.K.
[b] Composites Research Group, Faculty of Engineering, The University of Nottingham, Nottingham, NG8 1BB, U.K.
[c] Future Manufacturing Processes Research Group, The University of Leeds, LS2 9JT, U.K.

Abstract

3D printing of light-weight and mechanically-strong structures facilitates several applications. 3D printing of continuous carbon fibre reinforced polyetheretherketone (PEEK) presents exciting possibilities as the high stiffness and strength of the high-performance plastic PEEK reinforced with carbon fibre are paired with the agility of the 3D printing process. The Fused Filament Fabrication (FFF) process is used to print these parts, and a pultrusion system was designed and used to produce the filaments since they are not commercially available. This paper describes the design and construction of a pultrusion system within a wider project on carbon fibre reinforced PEEK FFF printing. This system is then used to produce the FFF filament with pultrusion speed and temperature optimisation.

Keywords: Additive Manufacture, Fused Filament Fabrication, feedstock production, continuous carbon fibre PEEK printing, composites printing.

1. Introduction

3D printing of polymer composites has the potential to improve significantly the material characteristics compared to those obtained from the conventional printing of pure polymers, by combining the matrix and reinforcements to achieve better functional material properties [1]. For instance, in aerospace, automobile and construction industries, 3D printing has been applied in creating complex lightweight structures [2]. The outcomes of this research on carbon fibre with polyetheretherketone (PEEK) polymer has the potential to improve the mechanical properties available for 3D printed composite components in the aerospace industry [3]. Currently there are also many investigations into 3D printed parts made from carbon fibre reinforced polymers, however, there are not many publications on the application of PEEK as the matrix material [4]. The Fused Filament Fabrication (FFF) process is one of the most popular AM method due to its low cost and fast production speed [5]. When conducting FFF printing, the process parameters can influence the quality of the printed part. The effects of FFF processing parameters has been discussed by Stood *et al.* [6]. There are five important process parameters: layer thickness, orientation, raster angle, raster width and air gap. These parameters determine the tensile, flexural and impact strength of the printed specimen. A study was conducted to evaluate the mechanical properties of continuous fibre reinforced thermoplastic composites printed by a commercially available Mark One printer [7]. In another study, in-situ fibre impregnation was adopted to print continuous fibre based composites [10, 11, and 12]. Matsuzaki *et. al.* [10] reported that the tensile modulus and strength of 3D-printed continuous carbon fibre reinforced PLA composites were about five times more than the tensile modulus and strength of the pure PLA specimens. This mechanical improvement is much larger compared to what can be achieved with short fibre reinforced PLA composites. However, in some cases, irregularity and discontinuity of fibre still happens. Although the mechanical properties of composites were largely improved compared to those of pure polymer, the improvement was still lower than the theoretical value calculated by the rule of mixture [9, 11]. For the FFF printing of carbon fibre with polymer, one of the likely disadvantages of co-extrusion is the poor mixing between matrix and fibres, therefore the volume fraction of carbon fibre of a printed parts has to be capped to a value

which is much lower than the theoretical maximum volume fraction [13]. One approach for making long fibre polymer feedstock for FFF printing was developed by Rietema [12]. In this approach, a feedstock material that already contained the fibre and matrix material was selected. A commingled yarn of E-glass and polypropylene filament was investigated. After the consolidation, the theoretical consolidation diameter could be achieved, meaning there was no or negligible void content. Vaneker's developed pultrusion apparatus for pre-processing the yarn contains a brass die with a central hole with a calculated diameter [14]. In the work of Eichenhofer *et al.* [15], 3D printer was combined with a customized extrusion process. The print head is combined with both pultrusion and extrusion so that the commingled yarns can be printed directly. This process is called Continuous Fibre Lattice Fabrication (CFLF). Nylon-12 was used as the matrix.

Since no continuous carbon fibre PEEK FFF filament is commercially available, carbon and PEEK commingled fibres are selected. This type of fibres is a commingled strand which has a low bending stiffness. Therefore, it is difficult to extrude this material directly to a 3D printer nozzle, as the strand will buckle and jam the supply tube when it is pushed into the HotEnd by an extruder. Hence a pre-processing stage for the feedstock has been developed in order to convert commingled fibre into FFF 3D printing filament. This pre-processing stage will transform the commingled fibres into semi-stiff material which will be easier to print. Instead of extruding the printing material, an inverted extruding process is used, known as pultrusion as it involves pulling rather than pushing the material through the die. Commingled fibres are first pulled from a print head with a specially-designed nozzle as a die, and the resulting material is used as the feedstock for the 3D printer. Since PEEK is a difficult polymer to process compared with either Rietema's or Vaneker's materials in terms of processing temperature, rheological and crystalline behaviours during the solidification, in this project, based on the properties of selected commingled CF/PEEK, an experimental pultrusion system for this application is designed.

2. Functional Analysis and System Architecture

The architecture of the pultrusion system includes four modules: the support to hold the supply of commingled fibres; a heating system with the die to consolidate the commingled fibres, a traction system to pull the filament, and the final spool to store the filament and transfer it to a high temperature 3D printer. Figure 1 shows each of the modules of the pultrusion process. In the diagram the thick arrows symbolize the material flow and the thin arrows the function of each of the modules.

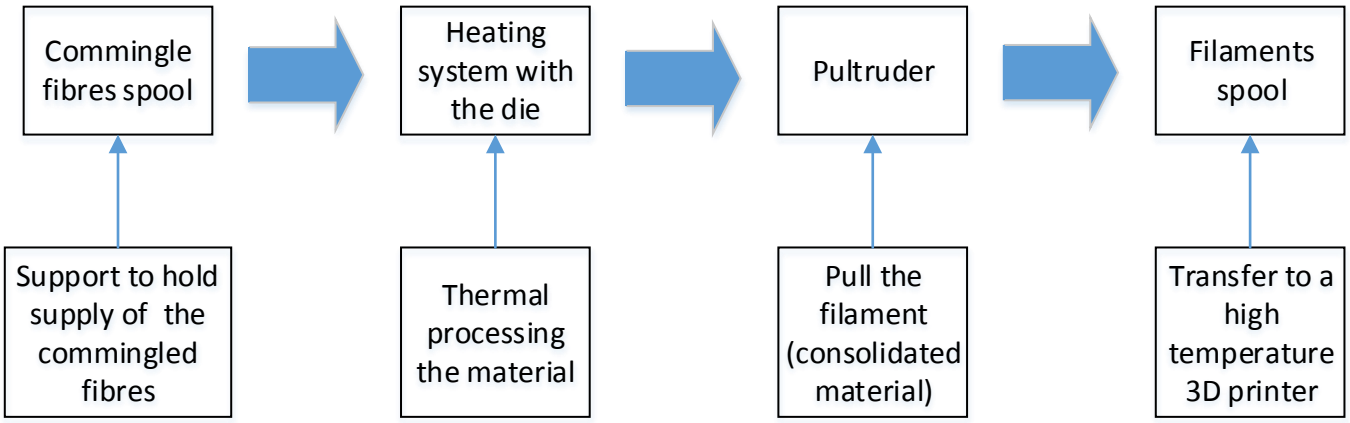

Figure 1: Pultrusion system diagram

The support of each of the modules, is designed such to keep the filament horizontally aligned during the process. An E3D high temperature HotEnd was used as the die heating system, and a specially designed die is used to replace the original nozzle. Different controllers control the temperature and stepper motors in order to have more flexible controlling during the experiments.

3. Conceptual Design and Its Evolution

The pultruder bracket assembly design has gone through several iterations. This pultruder includes a pulling wheel controlled directly by the stepper motor, and a pushing wheel which is in contact the pulling wheel and can be rotated by it. For ease of manufacture, both wheels were 3D printed with Acrylic material using OBJET printer [16], since two different components can be printed simultaneously in different proportions to create acrylic material with the desired elasticity. Hence, the outer rims of both the wheels are printed with a more rubbery material. On the running surface radial center line of the pulling wheel, a groove has been designed to work as a guide to keep the consolidated filament in the centre.

The third version, which is also the last version of the design for the pultruder assembly, introduced spacers on each side of the wheels to align two wheels better. It is built based on the previous version, which introduced a spring on the top in order to push the pushing wheel into contact with the pulling wheel. The first version of the pultruder assembly is shown in Figure 2 (a), with the aforementioned shortcomings in the design. The third instantiation of the pultruder which is also the current version is shown in Figure 2 (b).

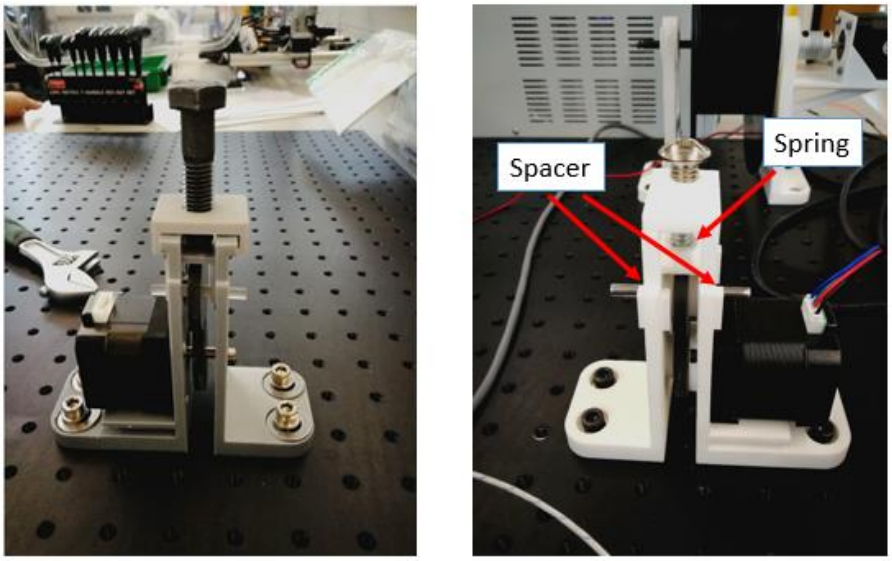

(a) First version pultruder (b) Third version pultruder

Figure 2. Pultruder Prototypes

4. The Calculation of the Pultrusion Die Diameter

The size of hole through the die is calculated based on the assumption of preservation of mass and density throughout the process. This ideal process does not exist in reality as small amounts of PEEK are leaking, and there is some degree of die-swell, also known as extrudate swell or Barus effect, which causes porosities during the process. First, the consolidation diameter is calculated. This is done with the following relation (1) [12]:

$$D = 2\sqrt{\frac{TEX}{\rho\pi}} \tag{1}$$

Where D is diameter of the consolidated filaments.

TEX is the linear mass of the commingled fibres, 307.7 TEX (g/km).

ρ = the density of the commingled fibres. Since ρ_{CF} = 1780 kg/m^3, ρ_{PEEK} = 1300 kg/m^3. With a volume fraction of carbon fibre of 57.4%, the combined density of the commingled fibres is then $\rho_{CF/PEEK}$= 1575.5 kg/m^3.

This yields a diameter of the consolidation filament of 0.4987 mm. The die can conveniently be made by machining a standard bolt (M6). Stainless steel has been selected as material for pultrusion die for its hardness prevents excessive wear of the die, to keep the diameter stable. A 0.5 mm diameter hole, 5 mm deep is drilled. The entrance has a diameter of 3.2 mm. The sizes of hole in the specially designed die are gradually reduced to 0.5 mm. In order to improve the efficacy of the die, the die keeps 0.5 mm diameter with a length of 5 mm. A cross section of the die nozzle is given in Figure 3.

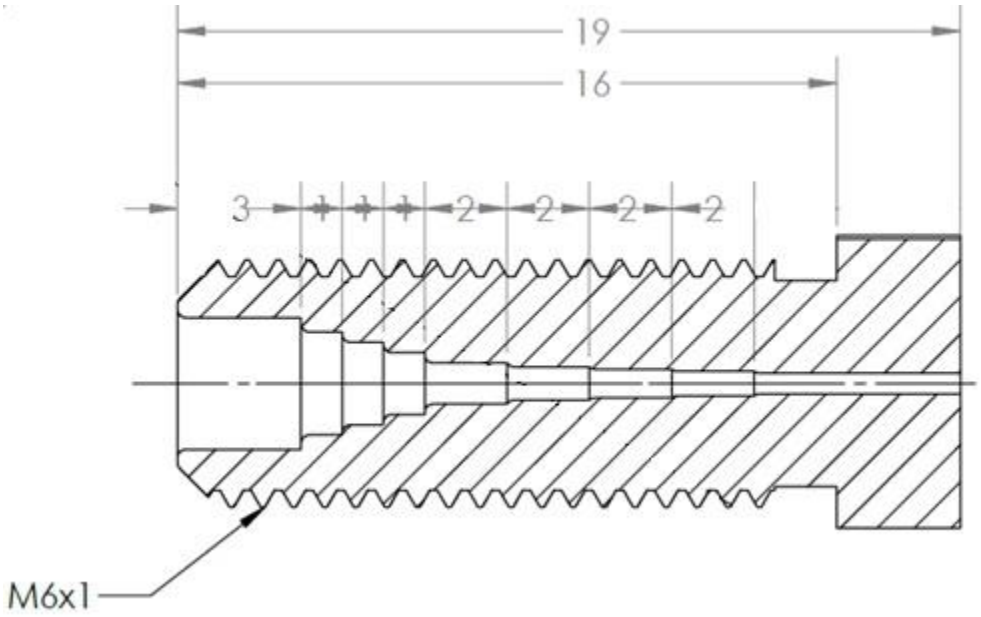

Figure 3: Cross section of pultrusion die

5. Further Detailed Design and Analysis

Before the mechanism design, a theoretical torque required to pull the commingled fibers has been calculated subject to the following assumptions: irrespective whether a pultruder or just a pulling wheel is used in the pultruder apparatus, the energy required to pull a length of material from the spool of commingled fibres through the pultrusion die is the same. As the power required to pull the commingled fibres through the die is independent from the power required to wind up the consolidated filament, these two powers can be superimposed onto each other and a bending moment of the filament can be used to estimate the required filament winding torque. In the system design, the rotation torque was calculated, then the minimum diameter shaft to apply tolerant this torque is calculated. Hence this section splits into two subsection.

5.1 Required Torque Calculation

The required torque for the winding spool actuation comes from the several forces and moments that are required for the processing in each of the modules discussed in Section 2. Further simplifying things, the pultruder is combined with the pulling spool wheel, because its required power can be easily related to the power required for the spool. In steady-state conditions, power for a rotating shaft is proportional to the torque and the rotational velocity:

$$P_{\text{rot}} = T\omega.$$

Furthermore, under steady-state conditions, power required for a system undergoing linear motion holds that it is proportional to the force and the linear velocity:

$$P_{\text{trans}} = Fu$$

For module 1 the contributions to the total are loaded the bending moment for the commingle fibres and the friction in the bearing. For module 2 it is the dry and wet friction in the die. For module 4 it is again the bending moment and the friction in the bearings. For ease of modelling, the commingle fibres can be considered a bundle of loose fibres and the consolidated material a strand of mixed fibres.

5.1.1 Friction in the Bearings Modules 1 and 4

There are two bearing pairs used in this pultrusion system. The first pair is utilized to support the spool with the commingle fibres, the other pair is for the pulling wheel. The diagram shown in Figure 4 helps to understand the calculation of bearing friction torque.

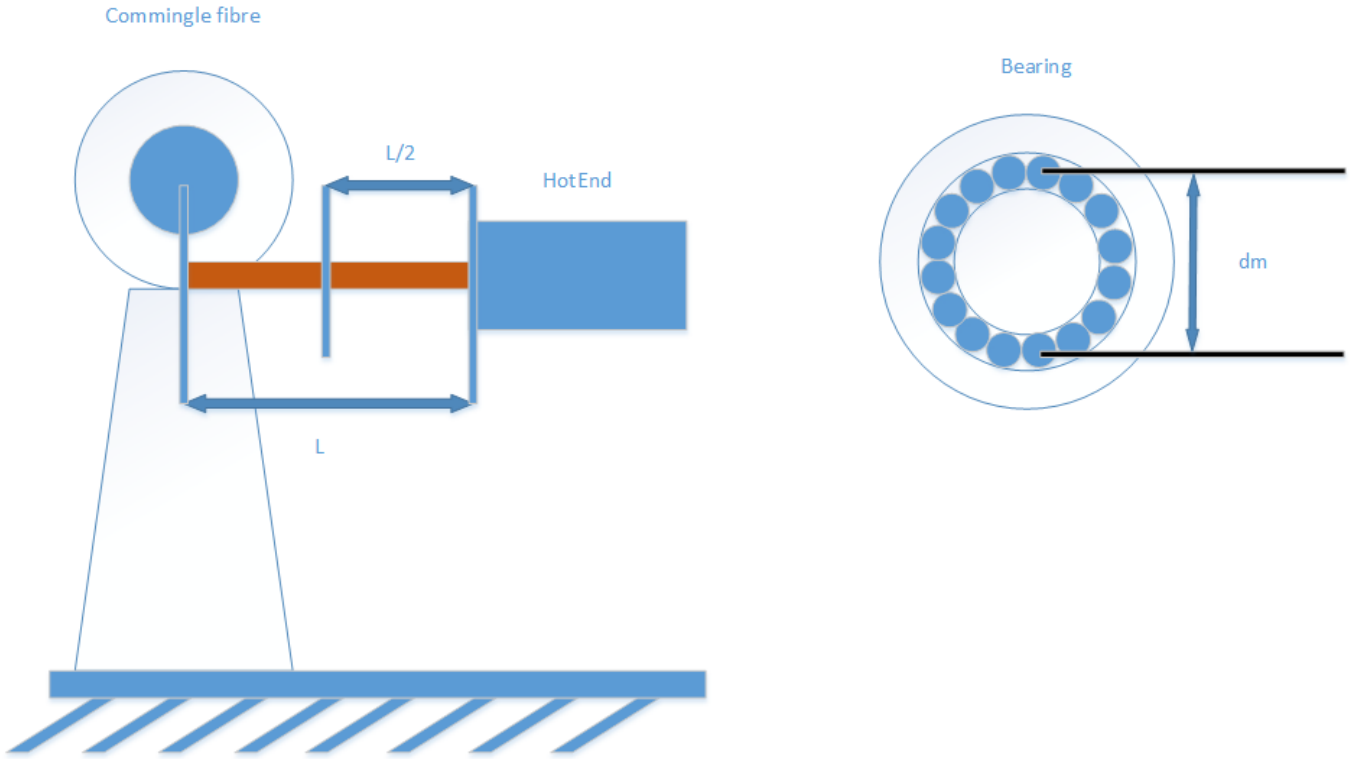

Figure 4: Diagram of friction moment for bearing calculation

For both sets, which include two times two bearings, the calculation of the frictional torque T_{bf} in the bearings is as:

$$T_{\mathrm{bf}} = 2m_{\mathrm{spool}}\mu\frac{d_m}{2}g$$

Where friction coefficient $\mu = 0.002$ for a standard ball bearing. m_{spool} is half of the material mass and further includes, shaft and wheel, which was assumed to be 0.5 kg, g is the gravitational constant and d_{m} is the pitch diameter in the bearings, see Figure 4.

5.1.2 Wet Friction in the Die

The value of $F_{friction}$ depends on the consolidated mixed material. The designed die nozzle, in this case, it is called die for the calculation. The length of the die is L_{die}, the diameter of the die is d_{die}. As shown in Figure 5.

Figure 5: Schematic showing the dimension of the consolidation die

As approximation, for the initial calculations, 8 mm was used as the length of the die. All the material data used, are taken from the Concordia Technical Data Sheet [17] and Victrex Data [18] as the material comes from these suppliers.

Assuming the carbon fibre is distributed evenly and the filament is completely consolidated after the pultrusion. The entropy increase in the system introduced by the processing makes that the fibres will be more randomly distributed than an equally spaced square or staggered distribution. A staggered distribution leads to an equilateral triangular unit cell, this is most compact form the fibres can be distributed. To allow for a larger average space, a square unit cell is assumed. It should be noted here, that the theoretical maximum fibre fraction is limited to touching fibres in the closest possible packing, namely 90.69%. The 57.4% volume fraction is well below that. Realistically, it can be assumed, as also later microscopy test showed, there will be regions in the cross section with a relatively high density of fibres and regions with a lower density. Taking a square unit cell represents a sort of worst case scenario. The unit cell (UC) concept is used, the space between the carbon fibres in this model is s. Since theoretically majority of the PEEK will be pulled along with carbon fibres, the shear stress should be caused mainly by the s distance of PEEK which is between the carbon fibre and inner side of the die. The schematic drawing of UC is shown in Figure 6. The blue part with radius of r is ¼ of carbon fibre and the white color is PEEK after consolidation from the die.

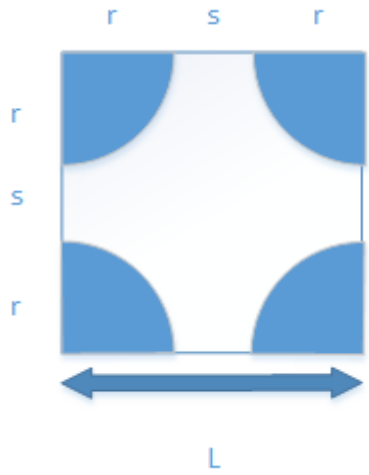

Figure 6: Unit cell of consolidated material

Based on simple geometric relationships, from this unit cell the inter fibre distance *s* can be worked out as follows:

$$L = 2\mathrm{r} + \mathrm{s}$$

$$A_{uc} = L^2 = (2r + s)^2 = 4r^2 + 4rs + s^2$$

$$A_{cf} = r^2\pi$$

Since,

$$A_{cf} = \phi A_{uc}$$

Then we get:

$$\frac{1}{\phi} A_{cf} = A_{uc}$$

Hence:

$$s^2 + 4rs + 4r^2 - \frac{r^2\pi}{\phi} = 0$$

Then s = 10.404^{-6}m is obtained. From the datasheet, the melt viscosity of PEEK 150G is $\mu_{PEEK} = 130\ \text{Pa} \cdot \text{s}$.

$$\tau = -\mu_{PEEK} \frac{\mathrm{d}u}{\mathrm{d}y} = -\mu_{PEEK} \frac{u_{\text{pultrusion}}}{\frac{1}{2}s}$$

So when the pulling speed is 5 mm/s, the shear stress $\tau = -1.2495 \times 10^7\ \text{N/m}^2$. With a die diameter of 0.5 mm, dictated by the theoretically specified consolidation diameter in Section 4 and a die length L_{die} of 8 mm, $F_{\text{friction,wet}} = -16.3363$ N.

5.1.3 Dry Friction in the Die

Taking standard dry friction based on the weight of the commingled fibres going through the die, the contribution is almost negligible, as the weight per unit length is low.

$$F_{\text{friction,dry}} = \mu_{\text{dry}} \frac{L}{2} A_{\text{cross}} \rho_{\text{comb}} g,$$

Where μ_{dry} is the dry friction coefficient, which is around 0.5 [19], $L/2$ is the half the length between the two spool, A_{cross} is the cross sectional area of the filament, ρ_{comb} is the combined density of the filament, see Section 4, and g is the gravitational constant. The total friction force, the sum of the wet and dry friction can be related to the load as seen by the actuated spool as:

$$T_{\text{friction}} = \left(F_{\text{friction,dry}} + F_{\text{friction,wet}}\right) \frac{d_{\text{spool}}}{2}.$$

5.1.4 Bending Moment

Following the usually safe assumption that the linear prediction for the bending moment results in a higher numerical value for the bending moment then applying plasticity and geometrically nonlinearity, a linear calculation for the bending moment represents the worst case scenario for the estimation of the bending moment. For beam bending there is the well-established linear relationship between bending moment M and radius of curvature ρ:

$$M = \frac{EI}{\rho},$$

Where E is the Young's modulus, also known as the modulus of elasticity, of the material and I is the second moment of inertia. The value ρ = 55 mm, the radius of the spool. The formula to calculate the second moment of inertia is:

$$I = \frac{\pi d^4}{64}.$$

For the loose case (module 1 in Figure 1), the bending moment is composed of the individual contributions of the individual fibres in the commingled fibres and for the filament it is the combined modulus of elasticity and the consolidated diameter that give the bending moment.

$$M_{\text{bending,loose}} = n_{\text{cf}} \frac{E_{\text{cf}} I_{\text{cf}}}{\rho} + n_{\text{PEEK}} \frac{E_{\text{PEEK}} I_{\text{PEEK}}}{\rho}$$

Where n_{cf} and n_{PEEK} are the number of carbon and PEEK fibres in the commingle fibres respectively. For the bending of the filament (module 4 in Figure 1), the following relationship describes the relation between the bending moment, the second moment of inertia, the combined modulus of elasticity and the radius of curvature:

$$M_{\text{bending,filament}} = (\phi E_{\text{CF}} + (1-\phi) E_{\text{PEEK}}) \frac{I_{\text{filament}}}{\rho},$$

Where ϕ is the carbon fibre volume fraction of 57.4%. For the bending moment at module 1, the bending $M_{\text{bending,loose}}$ is obtained as 0.0096 Nm, and in module 4, $M_{\text{bending,filament}}$ is 0.0193 Nm.

5.1.5 Force Requirement Extruder

The required torque is the total torque minus the bending of the filament, which includes $T_{friction}$ and T_{bf}. Based on the calculated required torque, the pulling force is obtained as -16.3326 N, which can be calculated as:

$$F_{pulling} = \frac{T_{required}}{r_{spool}} = \frac{T_{friction} + T_{bf}}{r_{spool}}$$

5.2 Minimum Shaft Diameter

In this section the minimum shaft diameter will be calculated based on failure due to shearing. Shear stresses in a shaft can occur due to being subjected torque and bearing loads.

5.2.1 Minimum Shaft Diameter Bearing Load

In Figure 7 a schematic of how the spool is attached to the support by the shaft is given. From this figure it can be seen that the shaft is in the so-called double shear condition, and the bearing load V is half the weight of the spool and commingle fibres or filaments. Using the standard calculation to find the average shear stress [20]; and equating the average shear stress to the maximum allowable shear stress, bearing load V to the half of the maximum weight of the spool and yarn, then the minimum shaft diameter can be calculated as follows:

$$d_{\text{shaft}} = \sqrt{\frac{4}{\pi} \frac{V}{\tau_{\text{max}}}} = \sqrt{\frac{4}{\pi} \frac{\frac{1}{2} mg}{0.5777 \sigma_{\text{y}}}} = 0.178 \text{ mm}$$

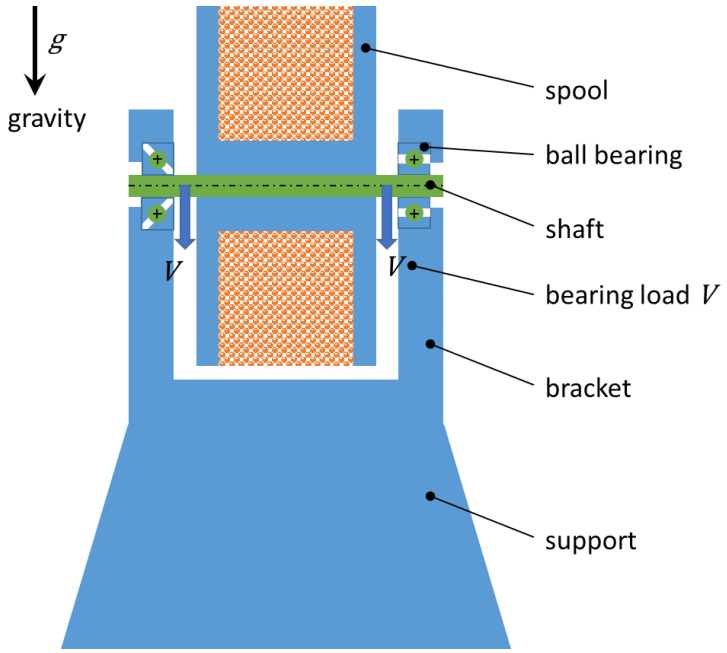

Figure 7: Schematic cross section of support and spool

5.2.2 Critical Load Case for Shaft Diameter

Since the minimum shaft diameter required to sustain the bearing load is smaller than that to sustain the twist due to torque, the twist is the critical load that governs the shaft diameter.

5.2.3 Minimum Shaft Diameter Twist

For the shaft selection, a steel shaft was selected. Based on the maximum torque calculated in the preceding section, the minimum shaft diameter based on the shear stress yield criterion can now be calculated. For the maximum shear stress the following relationship between torque and shear stress holds:

$$\tau_{\max} = \frac{TR}{J}, \tag{2}$$

Where R is the outer radius of the shaft and J is the polar moment of inertia. T is the total torque including $T_{friction}$, $M_{bending}$ and T_{bf}. For a solid shaft with circular cross-section the polar moment of inertia is defined as:

$$J = \frac{\pi R^4}{2}. \tag{3}$$

Substituting (3) into (2) gives:

$$\tau_{\max} = \frac{2T}{\pi R^3}. \tag{4}$$

The minimum shaft diameter can then be calculated from (5) as:

$$R = \sqrt[3]{\frac{2T}{\pi \tau_{\max}}}, \tag{5}$$

The maximum occurring shear stress $\tau_{\max}$ should be lower than the shear stress value for which plasticity occurs. The plasticity mechanism for shear due to twist is different than that of the plasticity occurring under a

tensile loading. The yield stress found in tensile tests for a material has been empirically related to the yield shear stress [18] to be:

$$\tau_{max} = 0.5777 \times \sigma_y$$

σ_y is 340 – 1000 MPa for steel. The worst case is taken by using the yield stress as 340 MPa in the calculations. With the torque calculated in the preceding section, the minimum diameter of the shaft is 2.9 mm. With a safety factor and for ease of assembly, a diameter of 6 mm was adopted in the design.

6. Final Pultrusion System Design and Assembly

The brackets and supports are designed to keep the spool, the loose commingled fibres and filaments levelled horizontally. The 3D CAD drawings of each of the supports are shown in Figure 8.

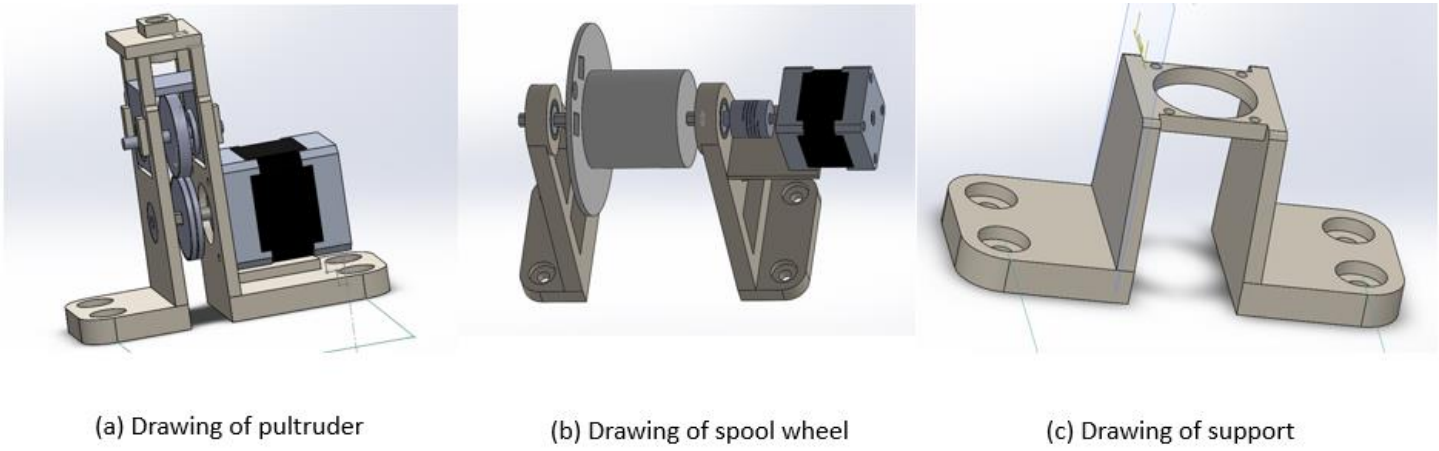

Figure 8: Drawing of pultrusion system supports

All the parts are 3D printed either by SLS process with nylon, FFF process with PLA of jetting process with acrylic. Based on the above design, the pultrusion system setup is shown as in Figure 9.

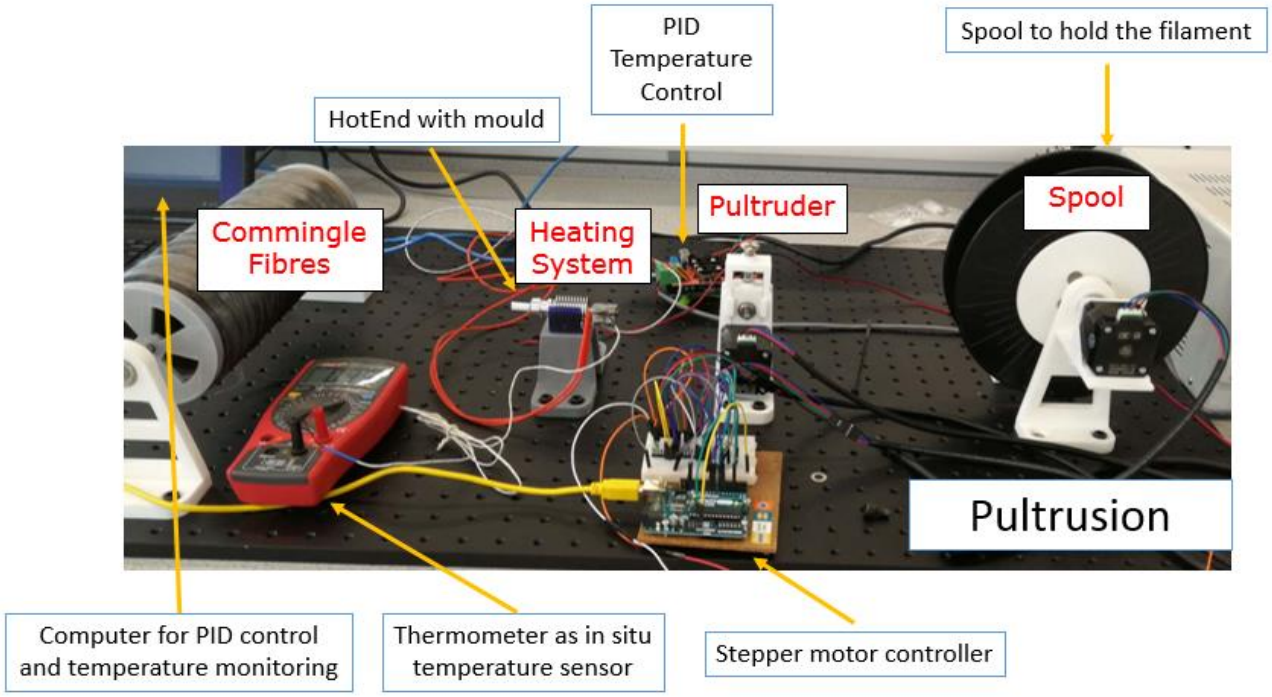

Figure 9: Final pultrusion system setup

7. Electronics and Controller Setup

For the temperature control, an Arduino Mega 2560 board and RAMPS 1.4 extension board are used. In this process, the RAMPS board is used for its MOSFET module. A PID control program is used for temperature control. A K-type thermocouple wire and associated amplifier board are connected via an analogue pin. The heating element is connected with a digital pin as it is driven using pulse width modulation to achieve an approximation to an analogue output. In the temperature control loop, the thermal sensor first detects the temperature, which is subsequently compared with the target temperature, after which it is decided if the heating element needs power input. While the computer can monitor the temperature through the controller board, a thermometer with K-type thermocouple is also used as in-situ temperature monitor. For the stepper motor control, A4988 stepper drivers were used to drive two NEMA 17 stepper motors with holding torque 0.44Nm, which is higher than the calculated total torque in section 5.2. The drivers are capable of microstepping and are set to 16 pulses per complete step in order to provide a high angular resolution of the stepper motors. When the system is running, the code is called to first heat up the die up to the target temperature. When this is achieved, the stepper motors can be started so that they pull the filament using the pultruder, and drive the take-up spool against the opposing torque from the tendency of the stiff filaments to uncoil.

8. System Evaluation, Conclusions and Future Work

32 processing conditions of parameter study on die temperature and pultrusion speed has been carried out with this pultrusion system. Quantitative measurement of filaments produced by the pultrusion system includes microscopy studies of both side view and cross sectional views in Figure 10 as one of the examples. Time-of-Flight Secondary Ion Mass Spectrometry (ToF-SIMS) was carried out for the initial penetration studies in order to identify different material in the cross-section. Density measurement and image processing were applied to find out how the processing condition effects the consolidation diameter, voids content, circularity, carbon fibre distributions of filaments. Results show the filament consolidation quality is temperature and pultruding speed dependent. When there is no material degradation under the safe process conditions, slower pultruding speed and higher die temperature result a better PEEK impregnation of carbon fibres in terms of less voids and more even carbon fibre distribution. The filament diameters are always larger than the theoretical consolidation diameter due to the relaxation of the PEEK during solidification. In the next step of the project, the filament has been used to print an actual part. Figure 11 below shows a single layer FFF CF/PEEK printed part with the CF/PEEK filament made under condition of pultrusion speed 0.5 mm/s and operation temperature 400 ˚C.

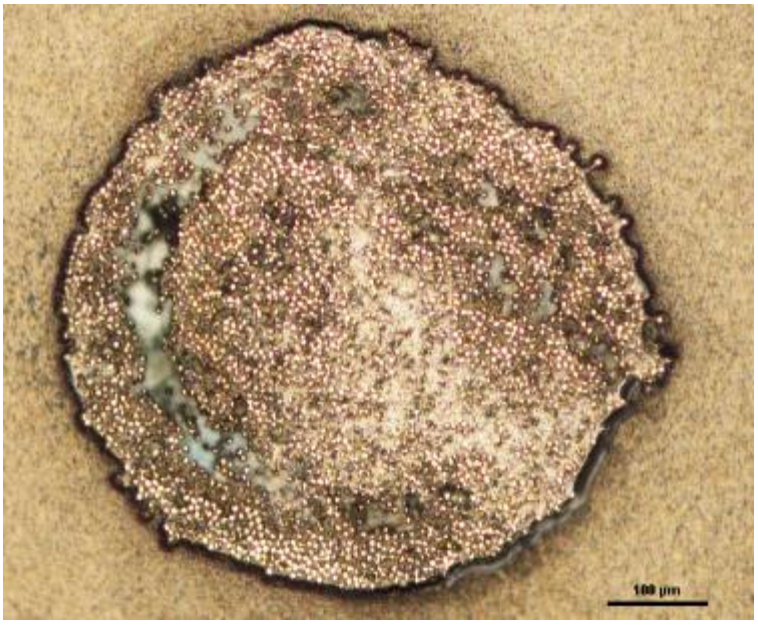

Figure 10: Cross sectional view of the pultruded filament under 0.5mm/s and 380˚C

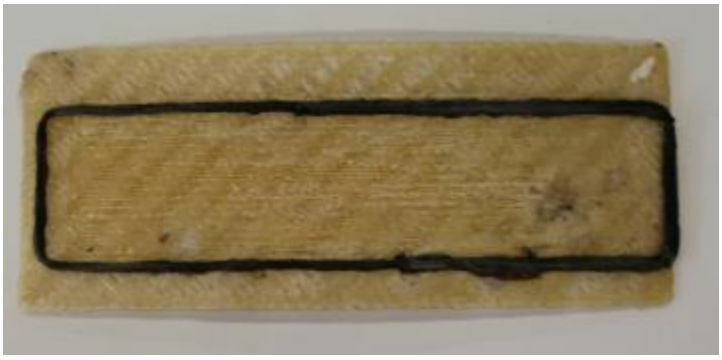

Figure 11. CF/PEEK printed part by a FFF 3D printer

Future work will focus on optimising printing process, by studying the weld formation, starting with a study of printing pure PEEK, to find out how the effective weld time affects the viscoelastic property of the PEEK printing. The second step will be to research the crystal growth of PEEK on carbon fibre under various weld durations. When an optimal method for the process of printing CF/PEEK material is established, design of FFF printing continuous and continuous fibre CF/PEEK parts can further unlock the potential of this material.

Acknowledgements

The first author would like to thank the China Scholarship Council (CSC) for the support of this project. Furthermore, the first author wishes to express her gratitude to Mr. Joe White, formerly of the University of Nottingham, who has greatly contributed to this work with his assistance building the building of her pultrusion system, and Dr. Ali Sohaib for sharing his sharing his invaluable insights into system design.

References

[1] Vivek, T., Arunkumar, P., Deshpande, A. S., Vinayak, M., Kulkarni, R. M., & Asif, A. (2018, April). Development of polymer nano composite patterns using fused deposition modeling for rapid investment casting process. In AIP Conference Proceedings (Vol. 1943, No. 1, p. 020110). AIP Publishing.
[2] Kroll, E., & Artzi, D. (2011). Enhancing aerospace engineering students' learning with 3D printing wind-tunnel models. Rapid Prototyping Journal, 17(5), 393-402.
[3] Denault, J., & Dumouchel, M. (1998). Consolidation process of PEEK/carbon composite for aerospace applications. Advanced Performance Materials, 5(1-2), 83-96.
[4] Wang, X., Jiang, M., Zhou, Z., Gou, J., & Hui, D. (2017). 3D printing of polymer matrix composites: A review and prospective. *Composites Part B: Engineering*, *110*, 442-458.
[5] https://www.3dhubs.com/knowledge-base/selecting-right-3d-printing-process, Website, accessed on 31 may 2019.
[6] Sood, A. K., Ohdar, R. K., & Mahapatra, S. S. (2010). Parametric appraisal of mechanical property of fused deposition modelling processed parts. *Materials & Design*, *31*(1), 287-295.
[7] Van Der Klift, F., Koga, Y., Todoroki, A., Ueda, M., Hirano, Y., & Matsuzaki, R. (2015). 3D printing of continuous carbon fiber reinforced thermo-plastic (CFRTP) tensile test specimens. Open Journal of Composite Materials, 6(01), 18.
[8] Matsuzaki, R., Ueda, M., Namiki, M., Jeong, T. K., Asahara, H., Horiguchi, K., ... & Hirano, Y. (2016). Three-dimensional printing of continuous-fiber composites by in-nozzle impregnation. *Scientific reports*, *6*, 23058.
[9] Namiki, M., Ueda, M., Todoroki, A., Hirano, Y., & Matsuzaki, R. (2014). 3D printing of continuous fiber reinforced plastic. *Proceedings of the Society of the Advancement of Material and Process Engineering*, (45), 187-196.
[10] Tian, X., Liu, T., Yang, C., Wang, Q., & Li, D. (2016). Interface and performance of 3D printed continuous carbon fiber reinforced PLA composites. Composites Part A: Applied Science and Manufacturing, 88, 198-205.

[11] Van Der Klift, F., Koga, Y., Todoroki, A., Ueda, M., Hirano, Y., & Matsuzaki, R. (2015). 3D printing of continuous carbon fiber reinforced thermo-plastic (CFRTP) tensile test specimens. Open Journal of Composite Materials, 6(01), 18.
[12] Rietema, M. J. (2015). Design of a prototype machine for 3D printing with continious fiber reinforcement (Master's thesis, University of Twente).
[13] Li, N., Li, Y., & Liu, S. (2016). Rapid prototyping of continuous carbon fiber reinforced polylactic acid composites by 3D printing. Journal of Materials Processing Technology, 238, 218-225.
[14] Vaneker, T. H. J. (2017). Material extrusion of continuous fiber reinforced plastics using commingled yarn. Procedia CIRP, 66, 317-322.
[15] Eichenhofer, M., Maldonado, J. I., Klunker, F., & Ermanni, P. (2015, July). Analysis of processing conditions for a novel 3D-composite production technique. In 20th International Conference on Composite Materials.
[16] Object30 3-D Printer System Website: https://www.ece.ubc.ca/~leos/pdf/tools/objet/manual.pdf (accessed 30/06/2019)
[17] Concordia Fibers, (n.d.). Concordia Manufacturing LLC website: https://www.concordiafibers.com/, *private correspondence*.
[18] Victrex Datasheet PEEK 150G, (2017). Website: https://www.victrex.com/~/media/datasheets/victrextds150g-151g.pdf (accessed 14/06/2019)
[19] Rzatki, F. D., Barboza, D. V. D., Schroeder, R. M., de Oliveira Barra, G. M., Binder, C., Klein, A. N., & De Mello, J. D. B. (2015). Effect of temperature and atmosphere on the tribological behavior of a polyether ether ketone composite. Friction, 3(4), 259-265.
[20] Goodno, B.J., & Gere. J.M., Mechanics of materials. 9th Ed., SI / James M. Gere, Barry J. Goodno. ed. Boston, Mass., 2018. Print.